SUPPORTING INFORMATION

Near Infrared Fluorescent Nanoplatform for Targeted Intraoperative Resection and Chemotherapeutic Treatment of Glioblastoma

Derek Reichel[1], Bien Sagong[1], James Teh[1], Yi Zhang[2], Shawn Wagner[2], Hongqiang Wang[1], Leland W. K. Chung[3], Pramod Butte[1], Keith L.Black[1], John S. Yu[1],and J. Manuel Perez[1,2,3*]

[1]Department of Neurosurgery, Cedars-Sinai Medical Center, Los Angeles, CA 90048

[2]Biomedical Imaging Research Institute, Cedars-Sinai Medical Center, Los Angeles, CA 90048

[3]Samuel Oschin Comprehensive Cancer Institute, Cedars-Sinai Medical Center, Los Angeles, CA 90048

Corresponding Author

*Email: jmanuel.perez@cshs.org

SUPPLEMENTARY METHODS

HMC-Lys Synthesis

HMC-Lys dye was synthesized following a multi-step synthesis scheme (**Figure S1**). Intermediate products were collected at each step and characterized for identity and purity. Each step of the reaction scheme is described briefly below.

Synthesis of Indole-Sulfonate Intermediate 1

2,3,3-trimethylindolenine (1.980 g, 2.0 ml, 12.5 mmol) was reacted with 1,4-butanesulfone (1.700 g, 1.3 ml, 12.5 mmol) for 4 h at 120°C, and the reaction was allowed to cool to room temperature. The reaction product, a dark purple solid, was collected, redissolved in 10 ml methanol, added to 350 ml of ethyl acetate, and stored for 24 h at -20°C. After 24 h, the purple precipitate was collected by filtration, washed twice with ethyl acetate and then washed once with diethyl ether. The intermediate indole-sulfonate product (1) was collected (2.120 g, 57% yield).

Synthesis of Indole-Carboxylic Acid Intermediate 2

2,3,3-trimethylindolenine (7.000 g, 7.1 ml, 44.0 mmol) was reacted with 6-bromohexanoic acid (8.560 g, 44.0 mmol) overnight at 80°C. The reaction product was collected, evaporated at reduced pressure, redissolved in acetonitrile, added to 150 ml of ethyl acetate, and stored overnight at -20°C. The product, a purple precipitate, was filtered and then washed several times with diethyl ether. The intermediate indole-carboxylic acid product (2) was collected (2.020 g, 13% yield).

Synthesis of Dianaline Hydrochloride Intermediate 3

Phosphorous oxychloride (26.000 g, 15.8 ml, 170.0 mmol) was dissolved in DMF (18.0 ml, 237.0 mmol) and reacted for 30 minutes at 0°C to prepare a Vilsmeier reagent. Then, cyclohexanone (6.650 g, 7.0 ml, 67.8 mmol) was added dropwise to the reaction mixture, and the reaction was allowed to proceed at 100°C for 1 h. Following this step, aniline (12.60 g, 12.4 ml, 136.0 mmol) was diluted into 50 ml of ethanol, and the aniline-ethanol mixture was added dropwise into the reaction solution. The reaction was then allowed to proceed at room temperature for 1 h. After 1 h, the reaction mixture was added to hydrochloric acid solution (1 l, 6 N) and allowed to recrystallize overnight at 4°C. The crystals were collected by filtration, washed twice with cold water and then washed once with cold diethyl ether. The product was then reconstituted in 20 ml of methanol, added to 500 ml of hexane/tert-butyl methyl ether (1:1), mixed, and then

allowed to precipitate at room temperature for 4 h. The purified product was collected by filtration and washed 3 times with 1:1 hexane/tert-butyl methyl ether (1:1). The intermediate dianaline hydrochloride product (3) was collected (13.050 g, 55.4% yield).

Synthesis of Indole-Sulfate-Aniline Intermediate 4

Intermediate 1 (0.586 g, 1.98 mmol), intermediate 3 (1.070 g, 2.97 mmol) and sodium acetate (0.163 g, 1.98 mmol) were dissolved in 50 ml of ethanol and reacted for 2 h at 80°C. The reaction was monitored by thin layer chromatography (TLC, 4:1 chloroform:methanol, silicon dioxide plates) with an observed product peak (purple, R_f=0.7) and starting material peak (burgundy, R_f=0.0). After 2 h, the reaction was cooled to room temperature and evaporated under reduced pressure. The purple product was then redissolved in 10 ml of ethanol, added to 200 ml of acetone, sonicated and allowed to precipitate overnight at 4°C. The precipitate was filtered, rinsed 4 times with acetone, dried and collected. The intermediate indole-sulfate-aniline product (4) was collected (0.661 g, 64% yield).

Synthesis of HMC-Carboxylic Acid Intermediate 5

Intermediates 2 (0.635 g, 1.8 mmol) and 4 (0.941 g, 1.8 mmol) were dissolved in 70 ml of ethanol, sonicated, and reacted for 2 h at 80°C. The reaction was monitored by TLC (4:1 chloroform:methanol, silica) with an observed product peak (dark green, R_f=0.4) and starting material peak (purple, R_f=0.7). The reaction was halted when the starting product was entirely consumed. Following reaction completion, the reaction solution was cooled to room temperature and evaporated under reduced pressure. The red-brown precipitate was then redissolved in 10 ml of ethanol, added to 200 ml of diethyl ether, sonicated and allowed to form precipitates for 30 minutes at room temperature. The precipitates were then filtered, washed twice with diethyl ether, and redissolved in 10 ml of ethanol. The mixture was then added to a beaker containing ice water, stirred, and stored overnight at 4°C. The precipitates were filtered and washed 3 times with cold deionized water. The intermediate HMC-carboxylic acid intermediate (5) was collected (0.738 g, 60% yield).

Synthesis of HMC-Lys

Intermediate 5 (0.100 g, 0.142 mmol), DCC (0.032 mg, 0.156 mmol), and NHS (0.018 g, 0.156 mmol) were dissolved in 10 ml of anhydrous dichloromethane and reacted for 24 h at room

temperature. The reaction product was filtered and evaporated at reduced pressure, and then a solid layer was collected. Diethyl ether was added to the solid layer and briefly sonicated. The dark red product was then collected by filtration. Next, the product was dissolved in 3 ml of acetonitrile. Sodium borate buffer (3 ml, 0.1 M, pH 8.5) was added to the reaction mixture, and the mixture was sonicated. The reaction mixture was cooled to 4°C, and N-Boc-lysine (0.038 g, 0.156 mmol) was added to the mixture. The reaction proceeded for 24 h at 4°C, and the reaction solution was then heated to room temperature and evaporated at reduced pressure. The product was purified by flash chromatography (Isco CombiFlash Rf+ Lumen, C_{18} column, room temperature, 35 ml/min, 254 nm, major peak at 25.8 min) using gradient elution (A: water, B: acetonitrile; 0-5 min, 10% B, 5-20 min, up to 55% B, 20-26 min, 55% B, 26-31 min, up to 70% B, 31-39 min, 70% B, 39-42.1 min, up to 100% B, 42.1-49.8 min, 100% B, 49.8 min, down to 80% B, 49.8-56.3 min, 80% B). The purity of the collected product was further verified by TLC (4:1 acetonitrile:water, C_{18}, Rf=0.25). The Boc-protected HMC-lysine was freeze dried and redissolved in 6 ml of dichloromethane. Trifluoroacetic acid (2 ml) was added to the reaction mixture and reacted for 2 h at room temperature. The reaction was monitored by TLC (4:1 acetonitrile:water, C_{18}, Rf=0.05). Following the reaction, the product was evaporated under reduced pressure, reconstituted in 10 ml of dichloromethane, and then evaporated again under reduced pressure. The HMC-Lys product was then reconstituted in water, lyophilized and collected (0.017 g, 14% yield).

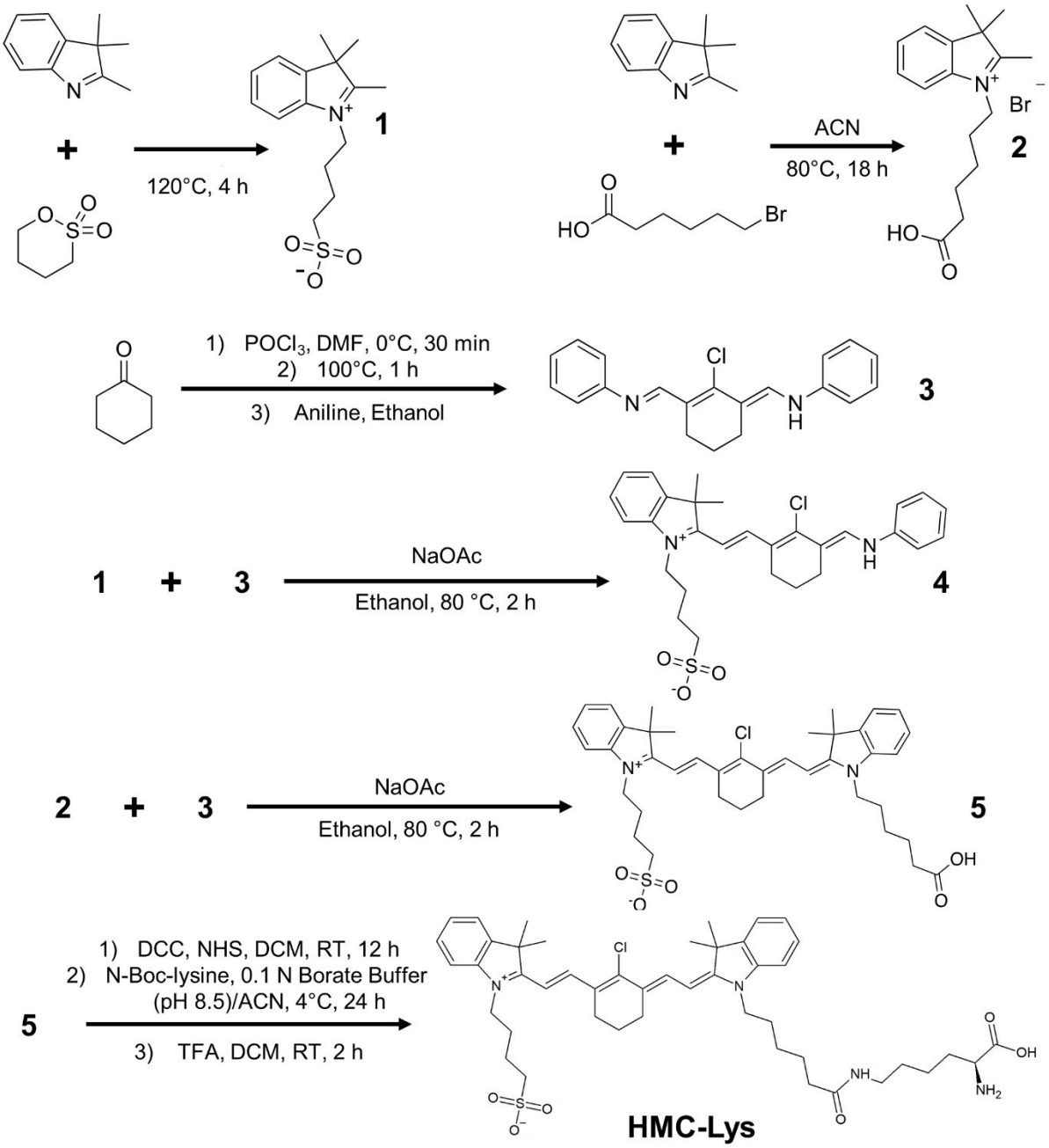

Figure S1. Synthesis scheme for HMC-Lys. HMC-Lys was prepared in a five step protocol. Reaction scheme intermediates are referred to by the numbers 1-5, which are listed to the right of their chemical structure.

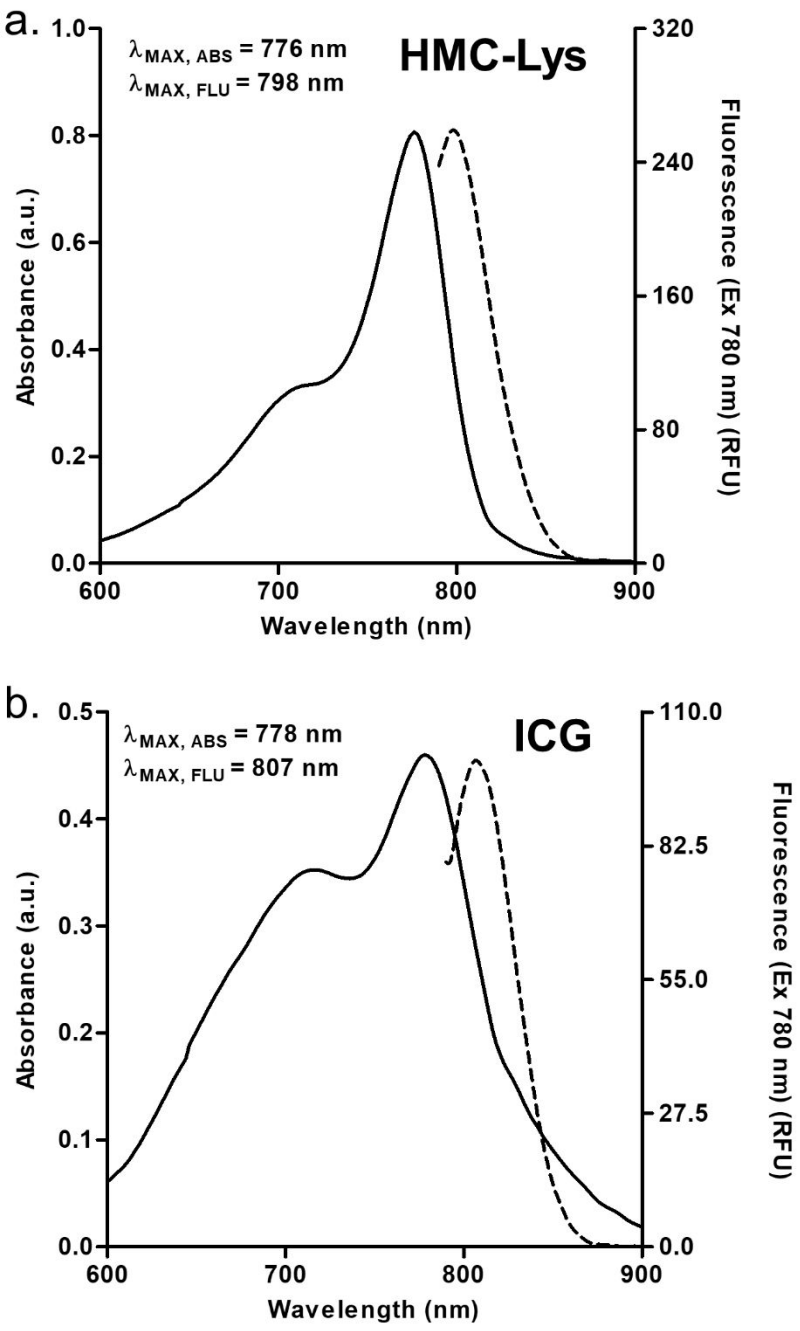

Figure S2. Optical properties of HMC-Lys (a) and ICG (b). Absorbance spectra (black lines) were measured at a 10 μM dye concentration in PBS, while fluorescence spectra (dashed lines) were measured at a 1 μM dye concentration in PBS to avoid dye quenching. HMC-Lys demonstrated stronger absorbance and fluorescence intensities at their maxima than ICG.

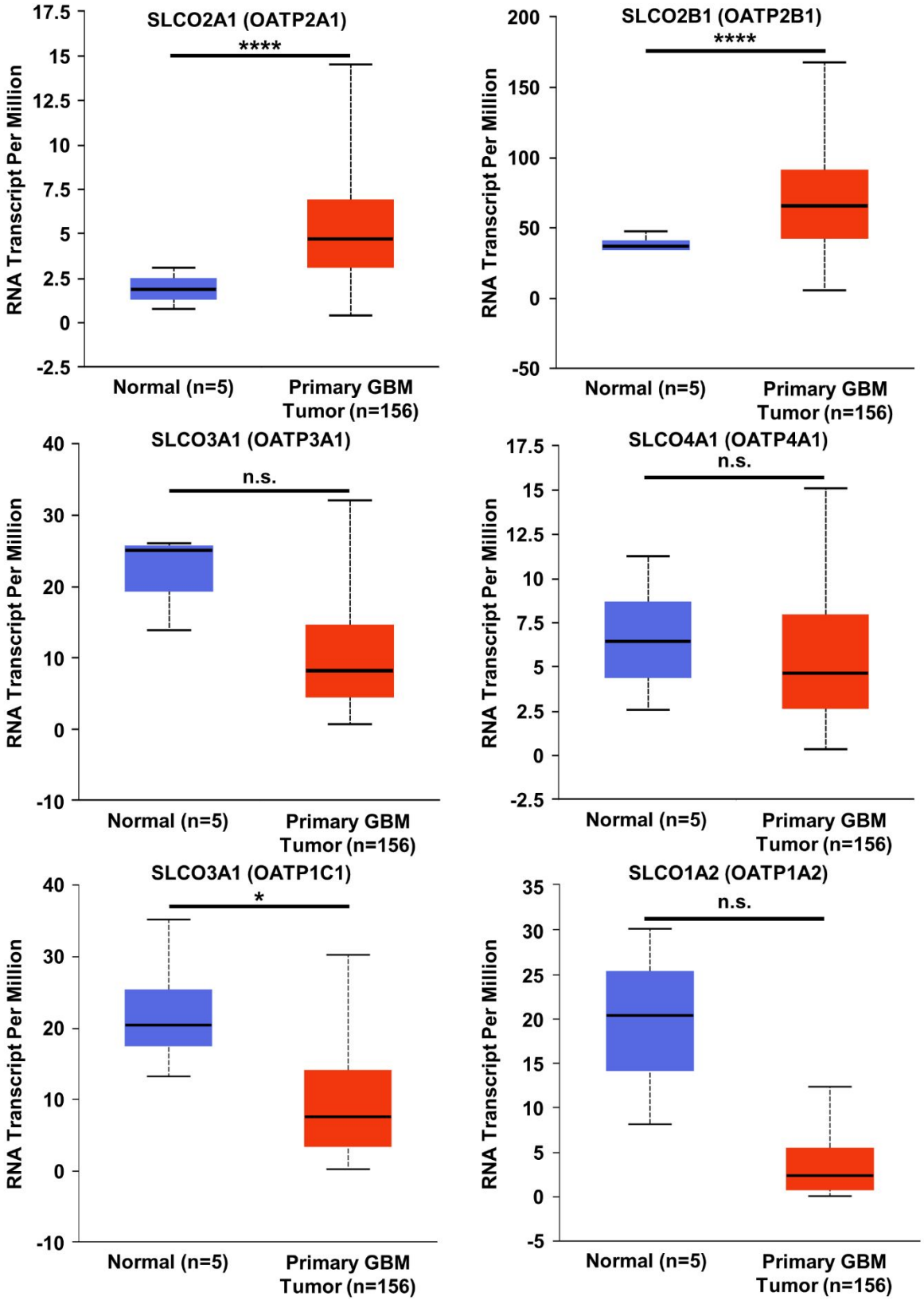

Figure S3. **RNA expression of various OATPs in normal brain and primary GBM tumor.** Data was collected from the UALCAN web portal searching the Cancer Genome Atlas.

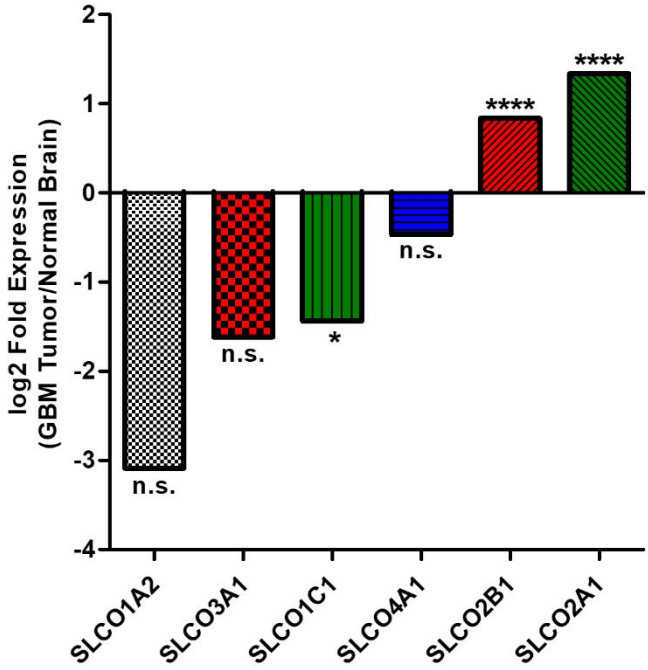

Figure S4. RNA expression ratios of OATPs in primary GBM tumors compared to normal brain tissue. Data was collected from the UALCAN web portal (Figure S2) and ratios were calculated using mean expression values. The statistical significance of each expression ratio was reproduced from UALCAN.

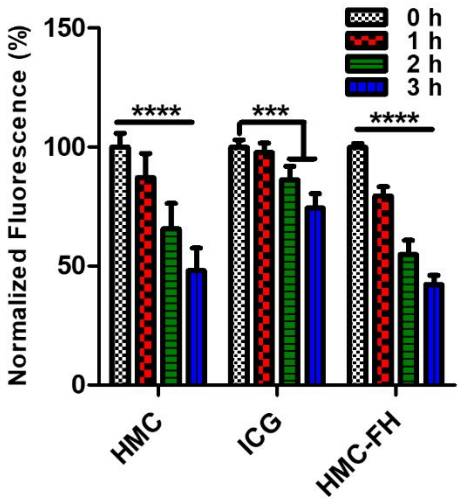

Figure S5. Fluorescence quantification of low concentration dye and nanoprobe samples under NIRF imaging conditions using the SIRIS camera. HMC and HMC-FMX lose about 50% of their NIRF signal after 3 h of continuous imaging, while ICG loses about 25% of its NIRF signal.

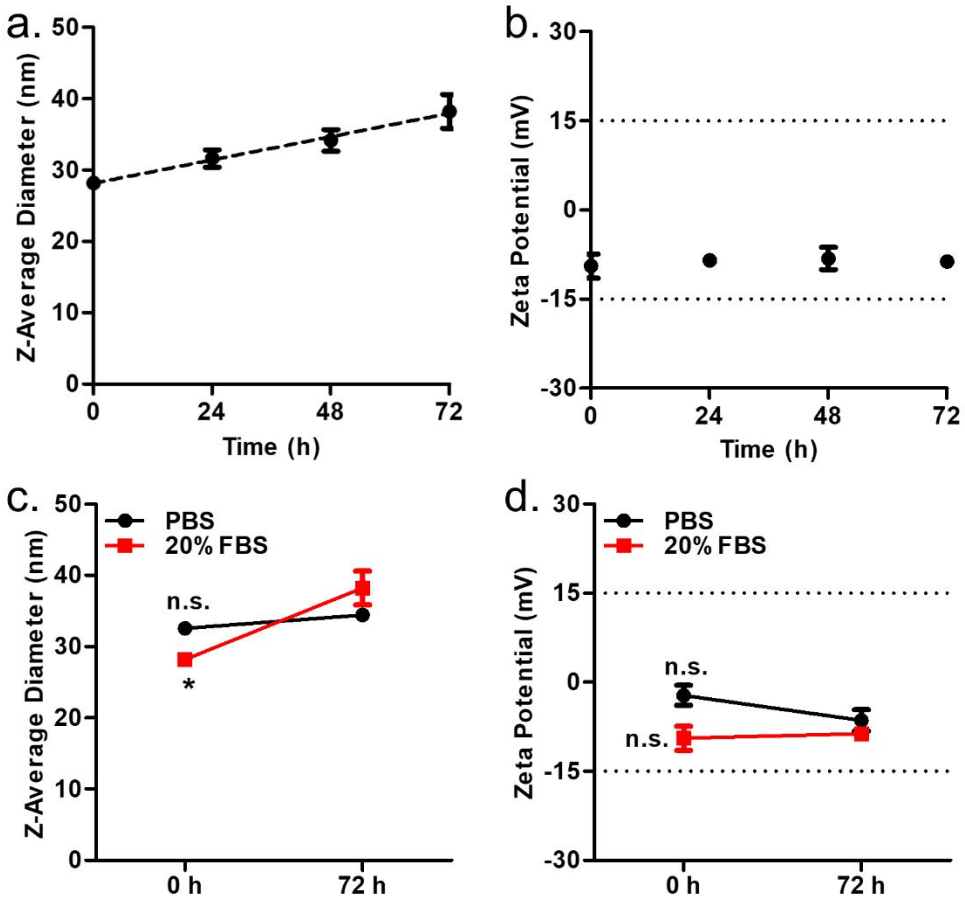

Figure S6. Serum effects on the physical-chemical properties of HMC-FMX. Although the diameter of HMC-FMX increased slightly over 72 h in 20% FBS (**a**), the surface charge remained neutral (**b**). The diameter and surface charge of HMC-FMX remained unchanged after 72 h in PBS (**c,d**). The dotted lines (**b,d**) represent the zeta potential range for a neutral surface charge (-15 to 15 mV).

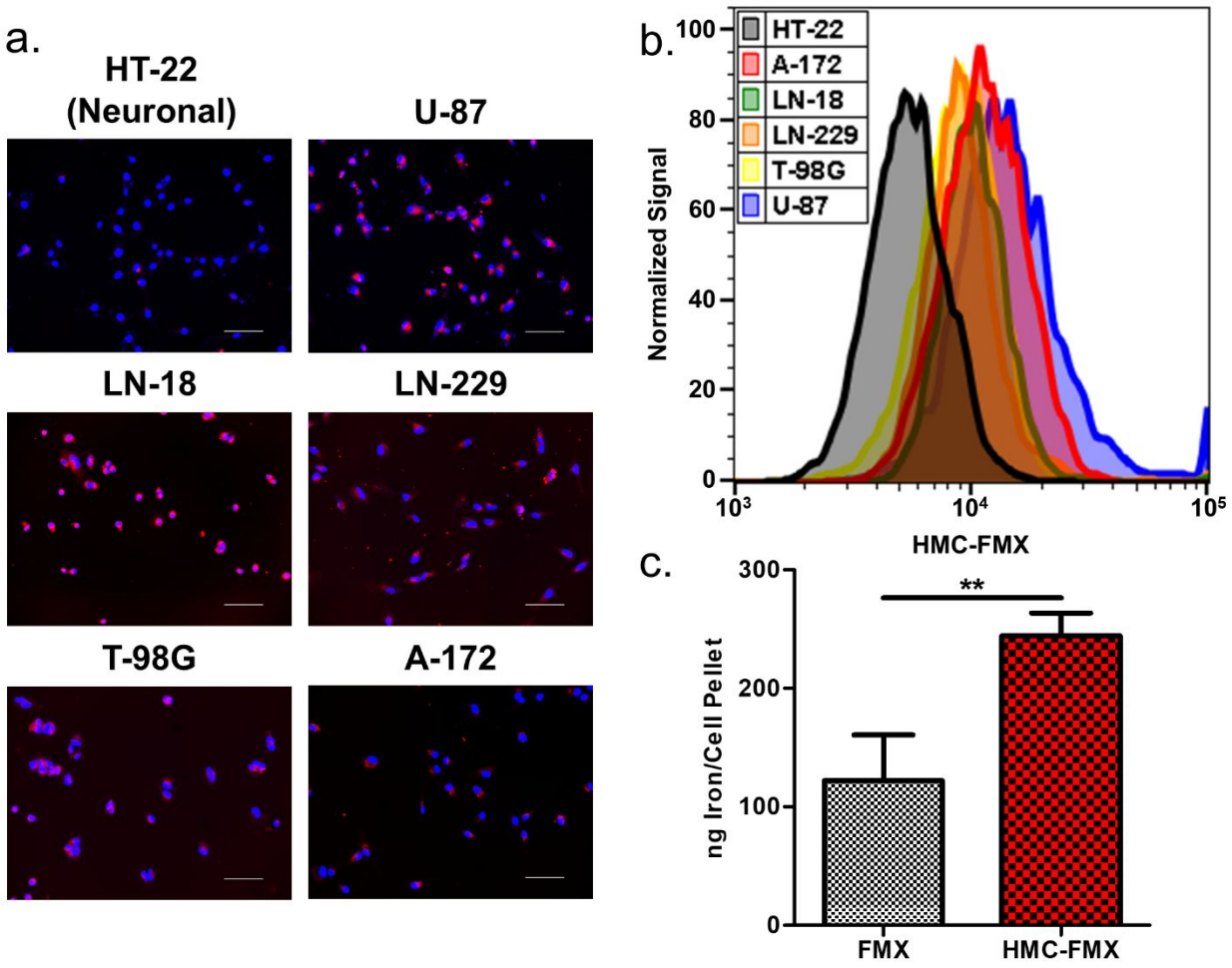

Figure S7. Cellular uptake of HMC-FMX is enhanced in GBM cells compared to neuronal cells. Fluorescence microscope images of HMC-FMX-treated cells (**a**). Images are taken at 20x magnification, and scale bars represent 100 μm. In the fluorescence images, blue represents nuclei and red represents HMC-FMX. Flow cytometry measurements of HMC-FMX-treated cells (**b**). Neuronal cell line HT-22 demonstrates decreased uptake compared to GBM cell lines. ICP-OES quantification of iron in cell pellets from FMX- and HMC-FMX-treated cells (**c**).

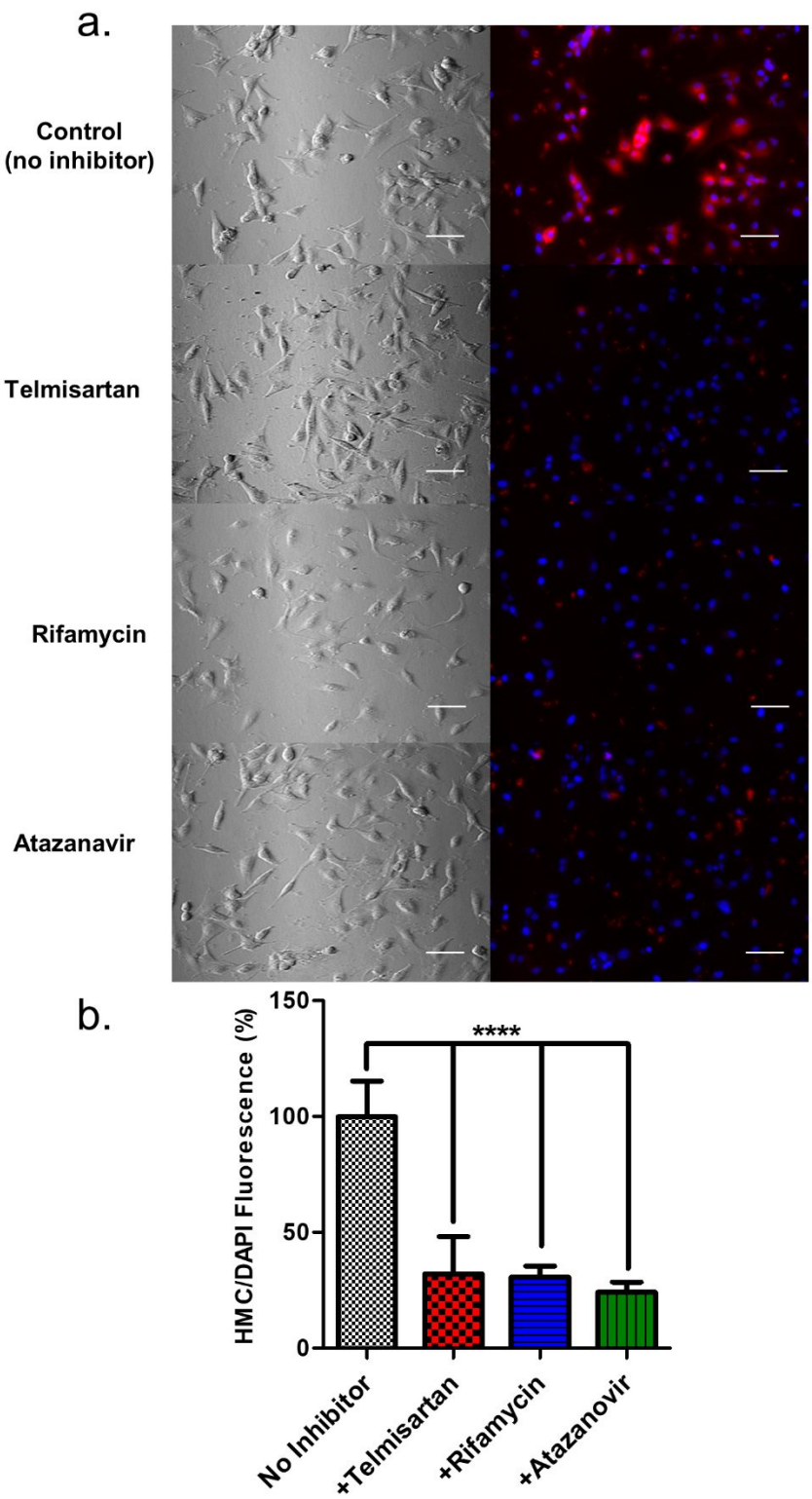

Figure S8. Effect of OATP inhibitors on HMC-FMX uptake. Cells were pre-treated with OATP inhibitors (telmisartan, rifamycin and atazanavir) and then treated with HMC-FMX. OATP inhibitors significantly reduced HMC-FMX uptake, indicating that HMC-FMX internalization is OATP-mediated.

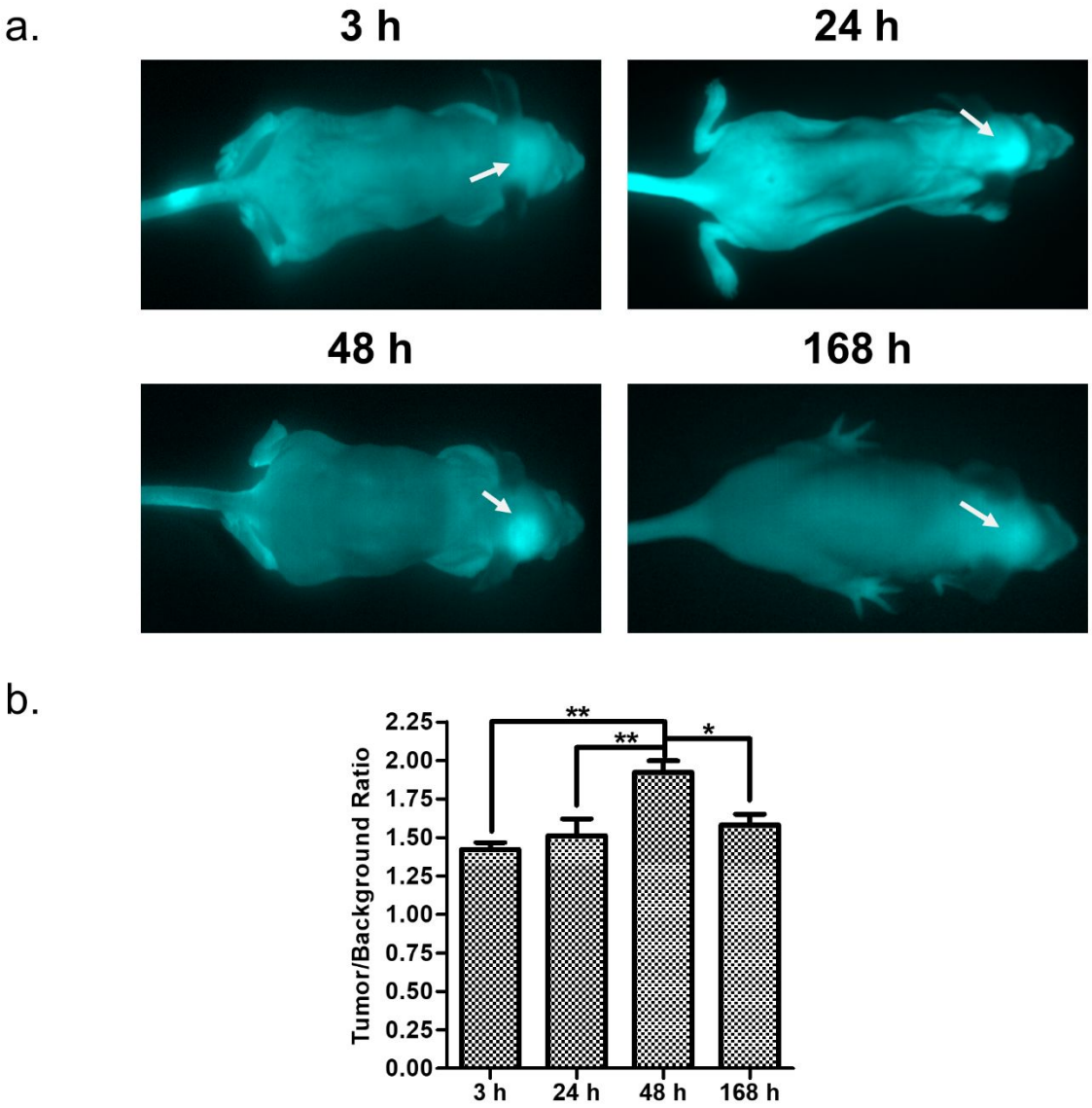

Figure S9. Fluorescence imaging of whole mice prior to organ removal. Arrows indicate the general location of brain tumors in mice (**a**). Quantification of fluorescence in brain tumor through the skull and skin relative to the back. The maximum signal was observed through the skull at 48 h post-injection (**b**).

Table S1. Physical-chemical and drug loading properties of HMC-FMX(PTX) and HMC-FMX(CDDP). Diameter changes following drug loading were not statistically significant. HMC-FMX(CDDP) had a slightly less negative zeta potential than other nanoprobes ($p<0.05$), but all nanoprobes were within the zeta potential range for a neutral surface charge (-15 to 15 mV).

Sample	Diameter (nm)	Zeta Potential (mV)	[Drug] (μM)
HMC-FMX	37.0 ± 3.0	-11.8 ± 0.3	-
HMC-FMX(PTX)	35.0 ± 2.9	-12.1 ± 0.5	301.8 ± 3.6
HMC-FMX(CDDP)	30.5 ± 1.6	-9.0 ± 1.3	1420 ± 10

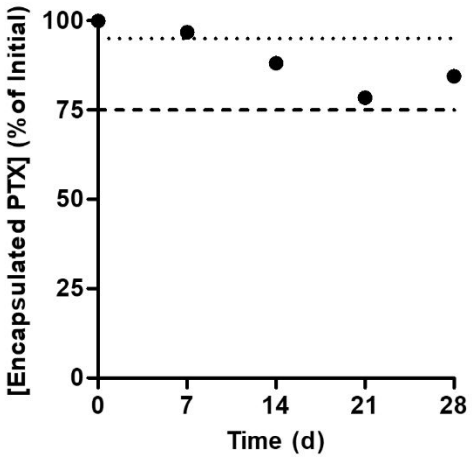

Figure S10. Drug encapsulation stability of HMC-FMX(PTX). PTX was selected as a model drug because encapsulated drug can be easily distinguished from precipitated released drug. PTX remains encapsulated (>75% of initial encapsulation) for up to 28 days during storage at 4°C. Lines indicate 95% (top, dotted) or 75% (bottom, dashed) of encapsulated drug remaining.

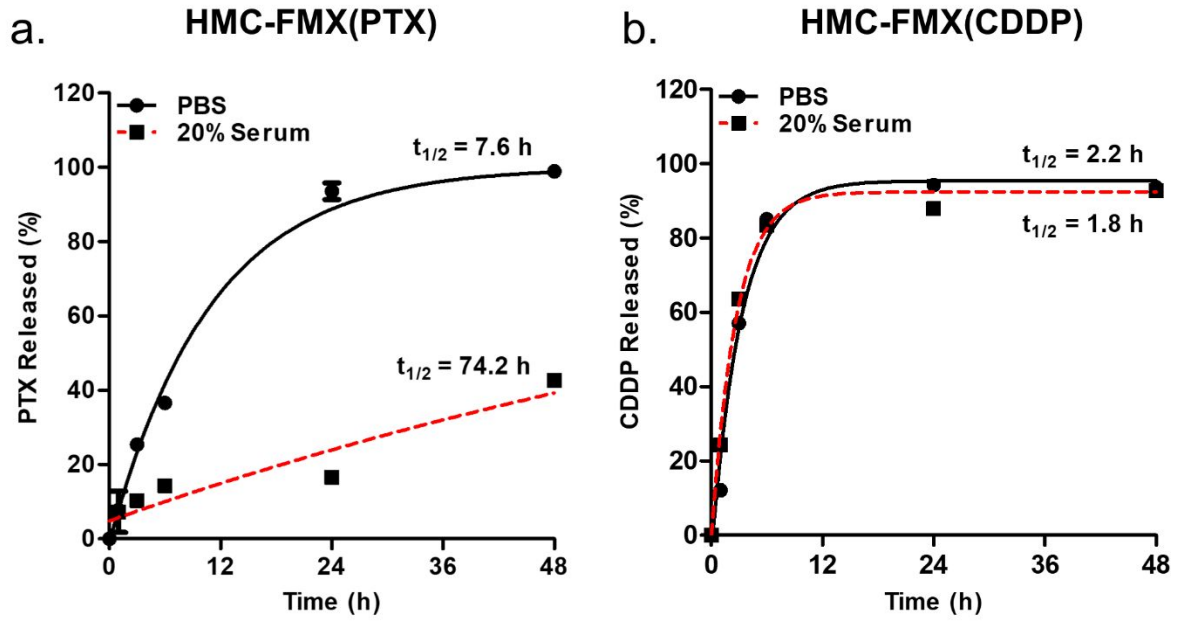

Figure S11. HMC-FMX nanoprobes demonstrate sustained drug release in serum. Drug release profiles of HMC-FMX(PTX) (**a**) and HMC-FMX(CDDP) (**b**) in PBS (solid lines) and 20% FBS (dashed lines). Drug release half-life differences are statistically significant for PTX ($p<0.0001$) but not CDDP ($p>0.05$).

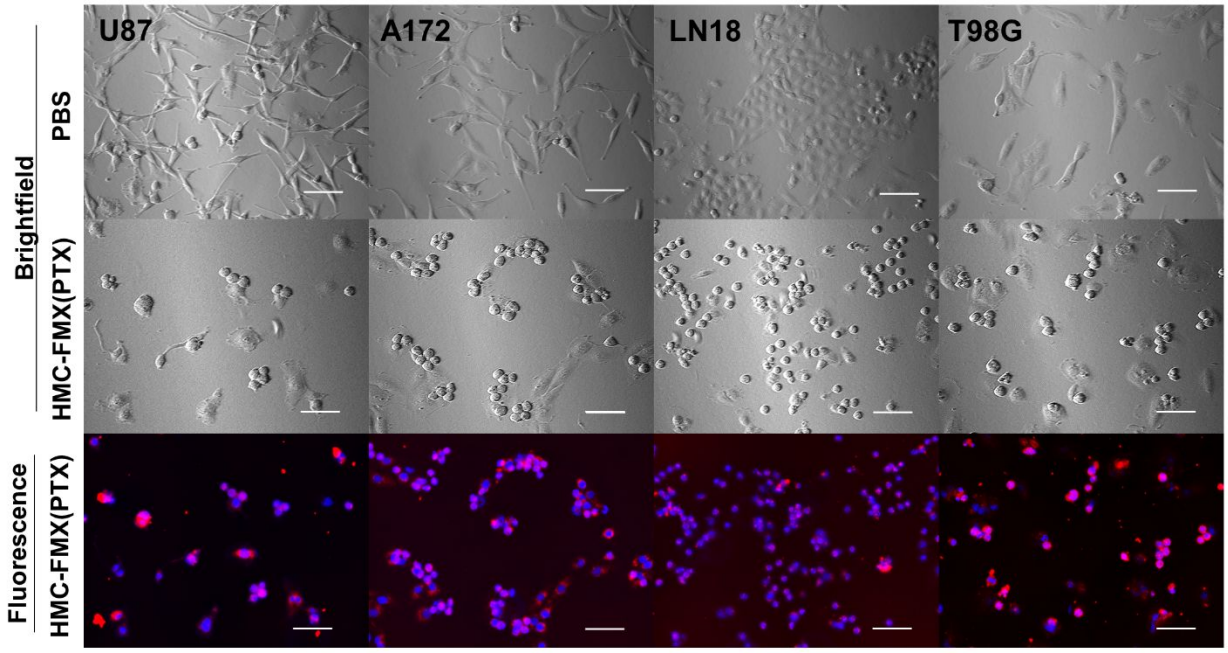

Figure S12. Drug-loaded HMC-FMX nanoprobes alter cell morphology following cellular internalization. Brightfield and NIRF microscope images of GBM cell lines treated with either PBS (top) or HMC-FMX(PTX) (middle and bottom) show visible changes in cell morphology (**a**). In these images, blue represents nuclei and red represents HMC-FMX(PTX). Scale bars are 100 μm.

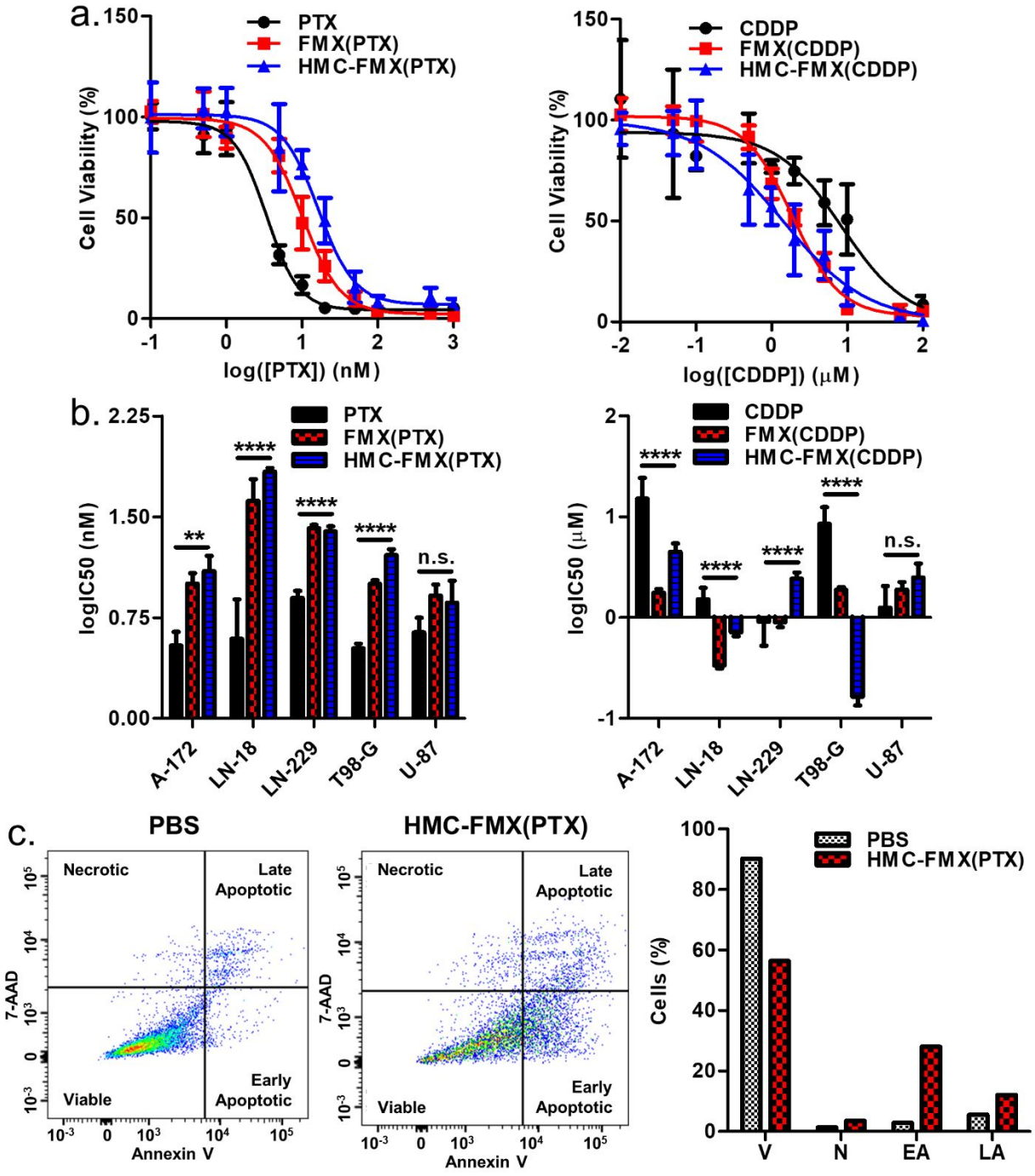

Figure S13. HMC-FMX nanoparticles reduce GBM cell viability *via* induction of apoptosis. Representative IC_{50} curves for T98-G cells (**a**). IC_{50} values of PTX-treated GBM cell lines were in the low nM range, while IC_{50} values for CDDP-treated GBM cell lines were in the low μM range (**b**). Nanoprobe encapsulation increased the IC_{50} of PTX but decreased IC_{50} of CDDP. Flow cytometry analysis (**c**) of PBS-treated (left) and HMC-FMX(PTX)-treated (middle) U-87 cells. A significant decrease in viable cells (V) was observed upon HMC-FMX(PTX) treatment, with a corresponding increase in the population of early (EA) and late apoptotic (LA) cells (right). No change was observed for necrotic (N) cells.

Table S2. IC_{50} values of PTX-, FMX(PTX)-, HMC-FMX(PTX)-, CDDP-, FMX(CDDP)-, and HMC-FMX(CDDP)-treated GBM cells. Results are presented as mean with 95% confidence intervals in brackets below.

	Cell Line				
Treatment	A-172	LN-18	LN-229	T98-G	U-87
PTX (nM)	3.4 [2.2-5.6]	3.9 [1.0-15.3]	7.9 [6.2-10.0]	3.4 [2.9-3.9]	4.4 [2.6-7.2]
FMX(PTX) (nM)	10.1 [7.1-14.3]	41.6 [19.7-88.0]	26.1 [23.4-29.2]	10.0 [9.0-11.3]	8.2 [5.6-12.1]
HMC-FMX(PTX) (nM)	12.5 [7.3-21.2]	68.7 [60.6-77.7]	24.7 [20.8-29.2]	16.4 [13.5-20.0]	7.3 [3.4-15.4]
CDDP (μM)	15.2 [5.9-39.0]	1.5 [0.9-2.6]	0.9 [0.3-2.7]	8.5 [4.0-18.4]	1.3 [0.5-3.4]
FMX(CDDP) (μM)	1.8 [1.5-2.0]	0.3 [0.3-0.4]	0.9 [0.7-1.1]	1.8 [1.7-2.1]	1.9 [1.3-2.7]
HMC-FMX(CDDP) (μM)	4.5 [3.0-6.6]	0.7 [0.6-0.8]	2.4 [1.8-3.2]	1.4 [1.0-2.1]	2.5 [1.3-4.7]

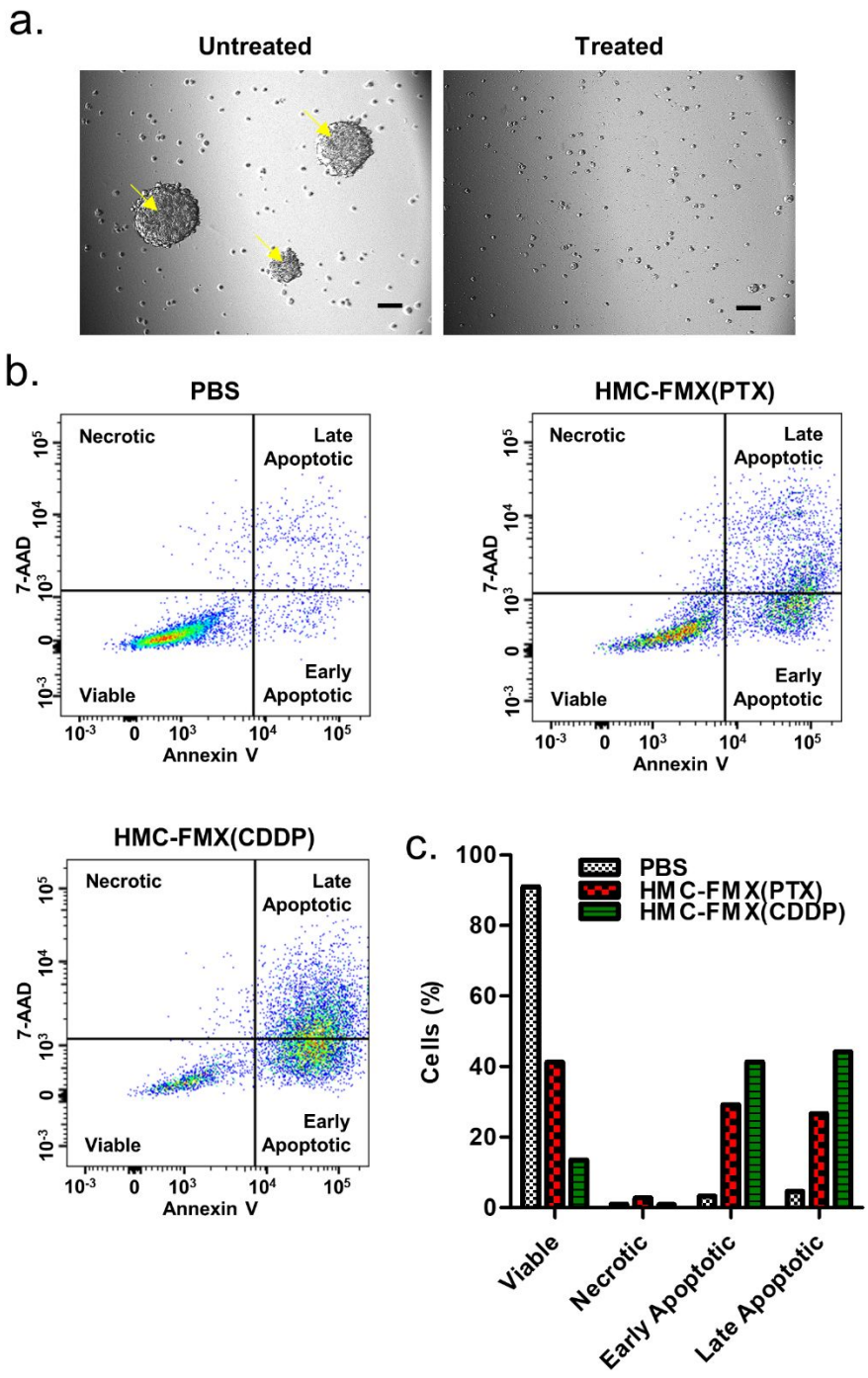

Figure S14. HMC-FMX nanoprobes target patient-derived GBM CSCs and label GBM CSC brain tumors in mice. Representative images of GBM cancer stem cell spheroids before (left) and after (right) nanoprobe incubation for 4 days (**a**). Note the disruption of spheroids after treatment. Flow cytometry analysis (**b**) of PBS- (middle left), HMC-FMX(PTX)- (middle right) and HMC-FMX(CDDP)-treated GBM CSCs (right). Treatment decreases the percent of viable cells and increase the percent of apoptotic GBM CSCs (**c**).

Table S3. Statistical comparison of tumor size by MRI monitoring following HMC-FMX(PTX) treatment.

Day	Comparison	Significance
0	HMC-FMX(PTX) *vs*. FMX(PTX)	n.s.
	HMC-FMX(PTX) *vs*. PTX	n.s.
	HMC-FMX(PTX) *vs*. PBS	n.s.
	FMX(PTX) *vs*. PTX	n.s.
	FMX(PTX) *vs*. PBS	n.s.
	PTX *vs*. PBS	n.s.
27	HMC-FMX(PTX) *vs*. FMX(PTX)	n.s.
	HMC-FMX(PTX) *vs*. PTX	n.s.
	HMC-FMX(PTX) *vs*. PBS	**
	FMX(PTX) *vs*. PTX	n.s.
	FMX(PTX) *vs*. PBS	**
	PTX *vs*. PBS	**
35	HMC-FMX(PTX) *vs*. FMX(PTX)	**
	HMC-FMX(PTX) *vs*. PTX	**
	HMC-FMX(PTX) *vs*. PBS	***
	FMX(PTX) *vs*. PTX	n.s.
	FMX(PTX) *vs*. PBS	n.s.
	PTX *vs*. PBS	n.s.
42	HMC-FMX(PTX) *vs*. FMX(PTX)	****
	HMC-FMX(PTX) *vs*. PTX	****
	HMC-FMX(PTX) *vs*. PBS	****
	FMX(PTX) *vs*. PTX	n.s.
	FMX(PTX) *vs*. PBS	**
	PTX *vs*. PBS	*

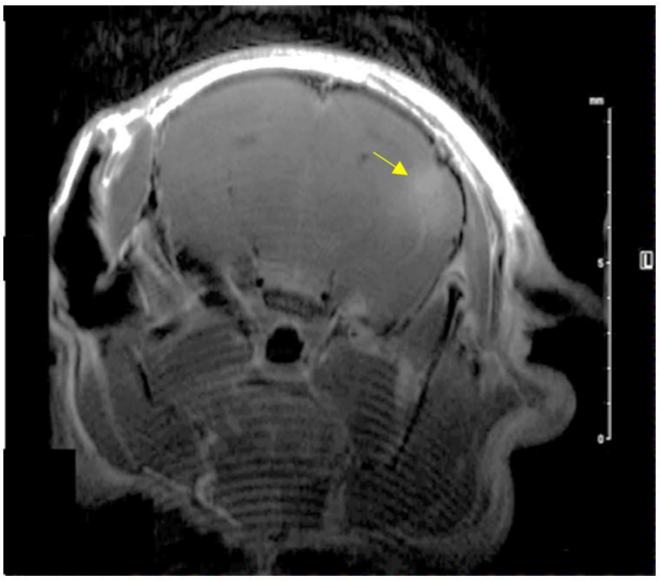

Figure S15. Representative brain MRI of an HMC-FMX(PTX)-treated mouse 50 days after intracranial injection. In this mouse, a small GBM tumor is observed (yellow arrow).

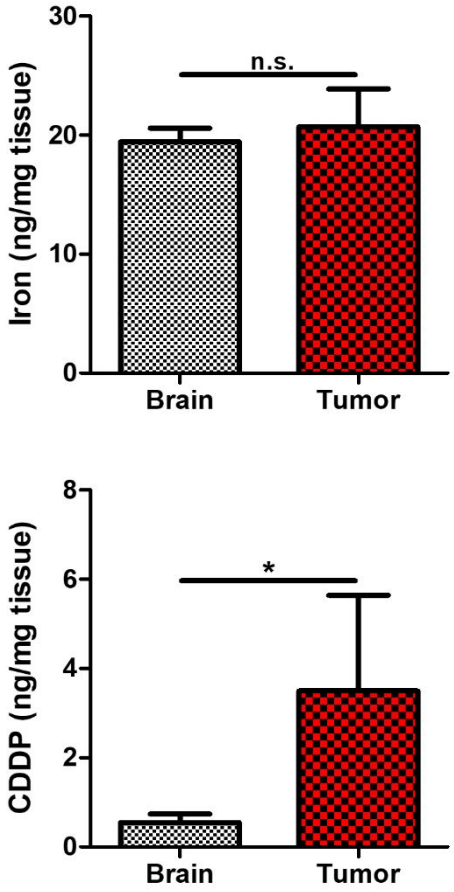

Figure S16. ICP-OES quantification of iron and CDDP in normal brain and brain tumors. While endogenous iron levels in tissue could not be easily distinguished from iron in FMX, CDDP was detected in brain tumors 48 h after treatment. CDDP was calculated based on platinum measurements.